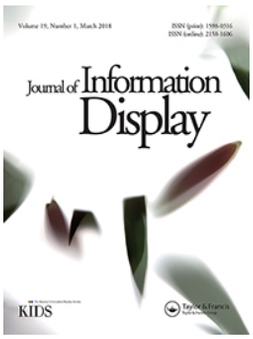

Journal of Information Display

ISSN: 1598-0316 (Print) 2158-1606 (Online) Journal homepage: https://www.tandfonline.com/loi/tjid20

Influence of A-site cation on the thermal stability of metal halide perovskite polycrystalline films

Himchan Cho, Joo Sung Kim, Young-Hoon Kim & Tae-Woo Lee

To cite this article: Himchan Cho, Joo Sung Kim, Young-Hoon Kim & Tae-Woo Lee (2018) Influence of A-site cation on the thermal stability of metal halide perovskite polycrystalline films, Journal of Information Display, 19:1, 53-60, DOI: 10.1080/15980316.2018.1424652

To link to this article: https://doi.org/10.1080/15980316.2018.1424652

Published online: 01 Feb 2018.

JOURNAL OF INFORMATION DISPLAY, 2018
VOL. 19, NO. 1, 53–60
https://doi.org/10.1080/15980316.2018.1424652

Taylor & Francis
Taylor & Francis Group

Influence of A-site cation on the thermal stability of metal halide perovskite polycrystalline films

Himchan Cho[a,c], Joo Sung Kim[a], Young-Hoon Kim[a,b,c] and Tae-Woo Lee[a,b,c]

[a]Department of Materials Science and Engineering, Seoul National University, Seoul Republic of Korea; [b]Research Institute of Advanced Materials, Seoul National University, Seoul, Republic of Korea; [c]BK21 PLUS SNU Materials Division for Educating Creative Global Leaders, Seoul National University, Seoul, Republic of Korea

ABSTRACT

This paper reports a comparative study of thermal stability between all-organic metal halide perovskite (MHP) $CsPbBr_3$ and organic–inorganic hybrid MHP (methylammonium lead bromide $MAPbBr_3$). The film morphology, crystal structure, steady-state photoluminescence intensity, and photoluminescence lifetime of $CsPbBr_3$ and $MAPbBr_3$ polycrystalline films were measured after thermal annealing at temperatures from 70°C to 230°C. The $CsPbBr_3$ films exhibited little change in their structural and luminescent properties after being annealed even at 230°C, whereas the $MAPbBr_3$ films exhibited a significant change in such properties due to their decomposition into $PbBr_2$ when annealed at $\geq$ 180°C. This study increased the understanding of the difference in the thermal stability of MHP polycrystalline films with different A-site cations.

ARTICLE HISTORY
Received 30 October 2017
Accepted 26 December 2017

KEYWORDS
Organic–inorganic hybrid perovskites; thermal treatment; decomposition; degradation; photoluminescence decay

1. Introduction

Metal halide perovskites (MHPs) have superior optical properties, such as high photoluminescence (PL) quantum efficiency (> 70% for colloidal MHP nanoparticles [1–5]), narrow emission spectrum (full width at half maximum < 20 nm [1,6]), and sharp absorption edge (low energetic disorder) [7,8]. Therefore, MHPs have been used in light-emitting diodes (LEDs) [1,6,9–17] and optically pumped lasers [18,19]. The most representative chemical formula of MHPs is ABX_3 (*A* is an organic ammonium, an alkali metal cation, or a mixture thereof; *B* is a metal cation (usually Pb^{2+}); and *X* is Cl^-, Br^-, I^-, or a mixture thereof) [1]. This ternary chemical structure enables the easy tuning of the optical properties (e.g. bandgap) of MHPs by controlling the molar proportions of their constituents; therefore, the emission color of MHPs can be easily tuned from blue to infrared by adjusting the ratio of the halide anions in them [10]. Also, MHPs have a much lower material cost than the conventional organic emitters (e.g. $Ir(ppy)_3$) and colloidal inorganic quantum dot (QD) emitters (e.g. CdSe/ZnS QDs). Furthermore, various solution processes can be used to fabricate MHP layers because MHP precursors are soluble in polar aprotic solvents (e.g. dimethylformamide, dimethyl sulfoxide (DMSO)).

Since the demonstration of MHP LEDs (PeLEDs) that are bright (> 100 cd m^{-2}) at room temperature (RT) [10,11], the electroluminescence (EL) efficiency of PeLEDs has been significantly improved [1–4,6,9,14–17,20,21]. High-efficiency methylammonium lead bromide ($MAPbBr_3$) PeLEDs (maximum current efficiency = 42.9 cd A^{-1}) have been achieved by suppressing the formation of luminescence quenchers and using nanocrystal pinning to fabricate pinhole-free $MAPbBr_3$ polycrystalline films with decreased grain size [9]. High-efficiency PeLEDs have also been achieved using Ruddlesden-Popper phase [12–15], interfacial layer engineering [10,21], and colloidal nanoparticles [2–4]. These achievements of high-efficiency PeLEDs demonstrated the great potential of MHPs as light emitters.

Despite the dramatic progress in EL efficiency, however, the stability of MHP materials and PeLEDs must be further improved. Particularly, the thermal instability of MHPs must be overcome because it limits the applicability of high-temperature processes that are often required to fabricate MHP films with high crystallinity [22]. Also, the large amount of heat generated by Joule heating or solar radiation in PeLEDs can degrade the MHP layers in them and may cause decoupling of the constituting layers at their interfaces [23].

CONTACT Tae-Woo Lee twlees@snu.ac.kr, taewlees@gmail.com Department of Materials Science and Engineering, Seoul National University, Seoul, Republic of Korea; Research Institute of Advanced Materials, Seoul National University, Seoul, Republic of Korea; BK21 PLUS SNU Materials Division for Educating Creative Global Leaders, Seoul National University, Seoul, Republic of Korea

ISSN (print): 1598-0316; ISSN (online): 2158-1606

Onset temperature T_{DEC} of thermal decomposition is lower in organic–inorganic hybrid (OIH) MHPs based on the MA^+ cations (e.g. $MAPbI_3$ and $MAPbBr_3$) ($\sim$220°C for $MAPbBr_3$) than in all-inorganic (AI) MHPs (e.g. $CsPbBr_3$; $T_{DEC} \sim$ 580°C) [24]; as such, OIH MHPs are more vulnerable to thermal stress than are AI MHPs. In practice, decomposition of MA-based OIH MHPs can occur at temperatures $< T_{DEC}$ (even at 85°C [25]). Therefore, AI MHPs ($CsPbX_3$) are promising alternative emitters for overcoming the thermal instability [6]. The influences of thermal stress on the structural and optical properties of $CsPbX_3$ polycrystalline films, however, have not been fully investigated compared with $MAPbX_3$, especially for Br-based MHPs.

In this work, the influence of A-site cation on the thermal stability of MHPs was investigated by comparing polycrystalline films of OIH MHP $MAPbBr_3$ and AI MHP $CsPbBr_3$. The changes in the film morphology, crystal structure, steady-state PL, and PL lifetime were observed and analyzed at different thermal annealing temperatures ($70 \leq T_{ANN} \leq 230$°C). This study provided a better understanding of how the structural and luminescent properties of these MHP polycrystalline films change with thermal stress.

2. Experiment

2.1. Preparation of $MAPbBr_3$ and $CsPbBr_3$ films

CsBr (99.999%, trace metal basis), $PbBr_2$ ($\geq$98%), and DMSO ($\geq$99.9%, anhydrous) were purchased from Aldrich. MABr was purchased from Dyesol. $MAPbBr_3$ precursor solutions (40.0 wt%) were made by mixing MABr and $PbBr_2$ in DMSO at RT while stirring (MABr:$PbBr_2$ = 1.05 : 1, mol:mol). $CsPbBr_3$ precursor solutions (10.4 wt%) were made by mixing CsBr and $PbBr_2$ in DMSO at RT while stirring (CsBr:$PbBr_2$ = 1.1 : 1, mol:mol).

MHP polycrystalline films were fabricated on glass or Si native wafer/self-organized conducting polymer (SOCP) substrates using the methods described elsewhere [6,9]. SOCP is made of poly(3,4-ethylenedioxythiophene): poly(styrenesulfonate) (PEDOT:PSS) (Clevios^{TM} PVP AI4083) and perfluorinated ionomer (PFI) with a PEDOT:PSS:PFI = 1:6:25.4 weight ratio [9]. Thereafter, the MHP layers were annealed at 70°C, 120°C, and 180°C for 10 min or at 180°C and 230°C for 30 min in a nitrogen atmosphere.

2.2. X-ray diffraction (XRD)

The XRD patterns of the MHP films (Si native wafer/SOCP/MHP) were measured in ambient conditions at RT using an X-ray diffractometer (D/Max-2500/PC, RIGAKU) operated at 40 kV and 100 mA (scan rate = 4° min^{-1}) to make Cu Kα radiation (wavelength = 1.54 Å).

2.3. Steady-state PL and time-correlated single-photon counting (TCSPC)

For use in steady-state PL and TCSPC measurements, the MHP films (glass/SOCP/MHP) were encapsulated with glass lids under a nitrogen atmosphere using a UV-curable resin, and were excited by 405 nm light sources. The steady-state PL of the MHP films was measured at RT using a spectrofluorometer (FP6500, JASCO). The PL lifetime of the MHP films was measured at RT using a TCSPC system [2] consisting of a picosecond-pulsed laser diode head (LDH-P–C-405B, PicoQuant), a TCSPC module (PicoHarp 300, PicoQuant), a monochromator (SP-2155, Acton), and a microchannel plate photomultiplier tube (R3809U-50, Hamamatsu).

3. Results and discussion

To investigate the thermal stability of $MAPbBr_3$ and $CsPbBr_3$ polycrystalline films, scanning electron microscopy (SEM) was used to observe the changes in the film morphology after annealing at T_{ANN} = 70°C, 120°C, 180°C, or 230°C (Figures 1 and 2). The MHP films were fabricated on the SOCP layers to create a uniform film morphology as reported in previous studies [6,9]. The $MAPbBr_3$ film without thermal annealing had a uniform fully covered morphology but also had numerous voids formed between the grains (Figure 1(a)). At T_{ANN} = 70°C or 120°C, the film morphology of the $MAPbBr_3$ films was improved; the grains were more closely packed without the voids than the grains without annealing were, and no thermal degradation was observed (Figure 1(b) and (c)). At T_{ANN} = 180°C, degraded areas appeared in 10 min (Figure 1(d)), and the film morphology completely changed to a non-uniform morphology with partial surface coverage in 30 min (Figure 1(e)); and at T_{ANN} = 230°C, the film morphology did not further change from that of the film annealed at 180°C for 30 min (Figure 1(e) and (f)), indicating that the degradation process was completed (note that the darker regions were the SOCP layers at the bottom of the $MAPbBr_3$ layer). This degradation is ascribed to the decomposition of $MAPbBr_3$ into $PbBr_2$, which follows one or both of the reaction paths shown below [26]:

$$CH_3NH_3PbBr_3 \rightarrow PbBr_2 + CH_3NH_2 + HBr \quad (1)$$

$$CH_3NH_3PbBr_3 \rightarrow PbBr_2 + CH_3Br + NH_3 \quad (2)$$

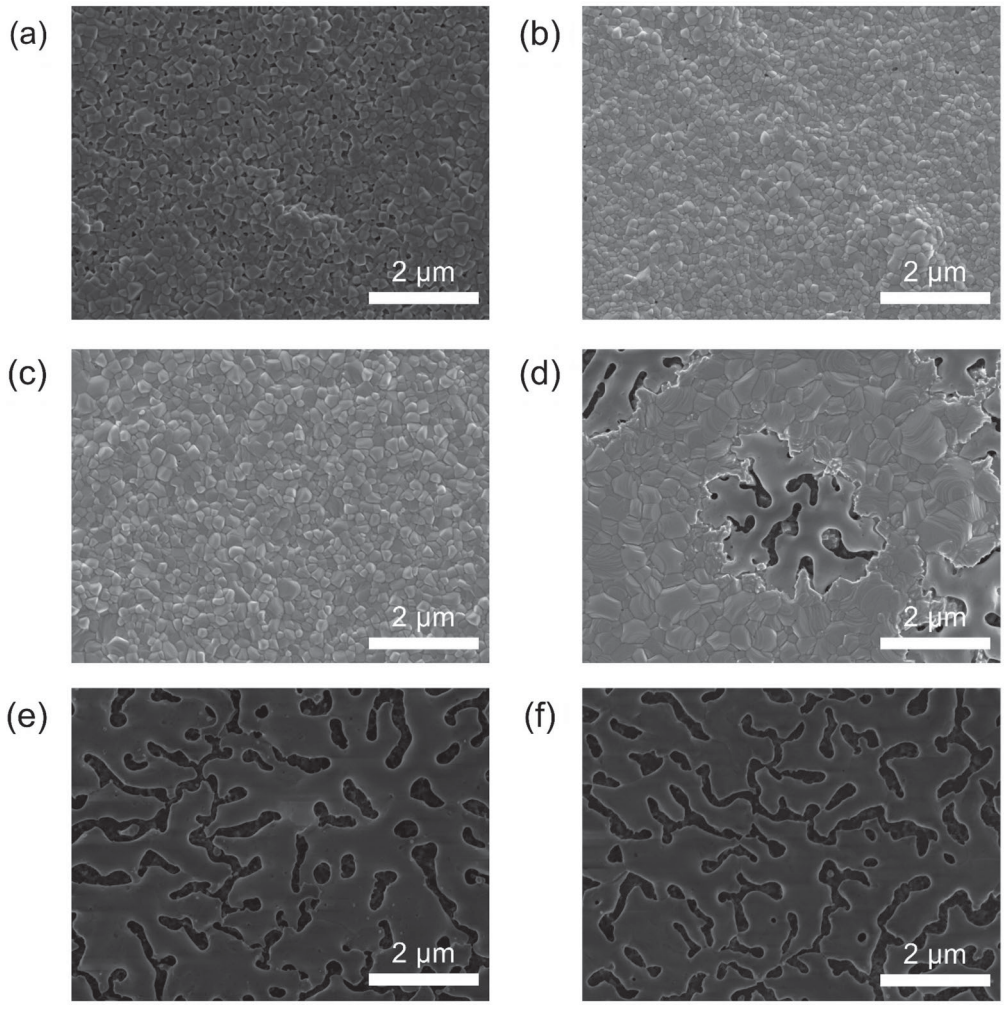

Figure 1. SEM images of the $MAPbBr_3$ polycrystalline films with different thermal annealing conditions: (a) without annealing; (b) annealed at 70°C for 10 min; (c) annealed at 120°C for 10 min; (d) annealed at 180°C for 10 min; (e) annealed at 180°C for 30 min; and (f) annealed at 230°C for 30 min.

The $MAPbBr_3$ grains were fused together with the adjacent grains during the decomposition into $PbBr_2$. This fusing effect is a result of Ostwald ripening [27] or coalescence [28]; both processes can be accelerated by high annealing temperatures (T_{ANN} = 180 or 230°C) and by the methylamine gas created during the decomposition. The increase in grain size with increasing T_{ANN} (from 70°C to 180°C) can also be explained by coalescence (Figure 1(b)–(d)) [28]. In contrast, the $CsPbBr_3$ polycrystalline films were thermally stable; the films annealed at 180°C and 230°C did not show any degradation in morphology (Figure 2). The high thermal stability of $CsPbBr_3$ films is attributed to (i) the absence of proton-donating organic constituents and decomposition reactions (1) and (2) and (ii) a positive enthalpy of the decomposition reaction of $CsPbBr_3$ [29].

To determine if the thermal stresses changed the crystal structures of the $MAPbBr_3$ and $CsPbBr_3$ films, the XRD patterns of the two MHP films with different annealing conditions were obtained (Figure 3; Tables 1–3). The $MAPbBr_3$ film annealed at 70°C showed 4 major XRD peaks at 15.02°, 21.26°, 30.20°, and 33.86°, which can be respectively indexed as (100), (110), (200), and (210) planes in cubic $Pm\bar{3}m$ phase (Figure 3(a), Table 1). The $MAPbBr_3$ films annealed at 180°C for 30 min exhibited XRD peaks from both $MAPbBr_3$ and $PbBr_2$; only the (100) and (200) peaks of $MAPbBr_3$ remained at the same positions as those in the film annealed at 70°C. This indicates that the $MAPbBr_3$ film annealed at 180°C for 30 min was not completely decomposed into $PbBr_2$ despite the complete change in its morphology (Figure 1(b)). The application of Bragg's law determined that the lattice parameter of $MAPbBr_3$ was 5.891 Å (Table 3). The $MAPbBr_3$ film annealed at 230°C exhibited a completely different XRD pattern, which matches well with the calculated XRD pattern of $PbBr_2$ (Figure 3(a) and (c)) [30]; this change confirms that the decomposition of $MAPbBr_3$ was completed by annealing at

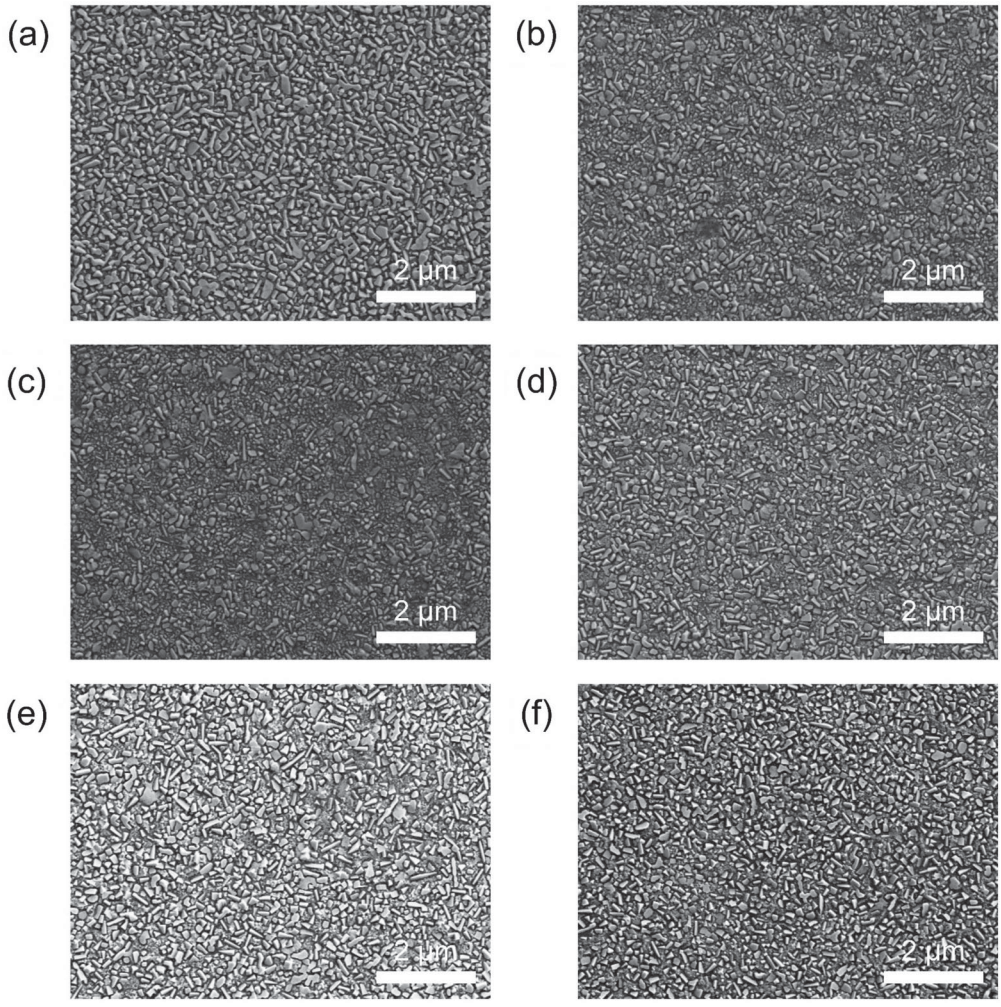

Figure 2. SEM images of the $CsPbBr_3$ polycrystalline films with different thermal annealing conditions: (a) without annealing; (b) annealed at 70°C for 10 min; (c) annealed at 120°C for 10 min; (d) annealed at 180°C for 10 min; (e) annealed at 180°C for 30 min; and (f) annealed at 230°C for 30 min.

230°C for 30 min. This temperature is slightly above the $T_{DEC} \sim 220$°C of $MAPbBr_3$ [24]. The occurrence of thermal decomposition at temperatures below the T_{DEC} of $MAPbBr_3$ (e.g. 180°C in this work) has often been reported [25,31,32].

The $CsPbBr_3$ films annealed at 70°C exhibited four major XRD peaks at 15.26°, 21.58°, 30.78°, and 37.9° (Figure 3(b), Table 2), which can be indexed as (101), (121), (202), and (321) planes in orthogonal *Pnma* phase [6,33]. In contrast to the $MAPbBr_3$ films, the $CsPbBr_3$ films annealed at 180°C and 230°C did not show dramatic changes in their XRD patterns compared with the $CsPbBr_3$ film annealed at 70°C. The calculated lattice parameters agreed with the previous reports (Table 3) [34]. Lattice parameters a and c slightly increased in the films annealed at 180°C and 230°C, whereas lattice parameter b slightly decreased (Table 3); the difference may be attributed to the lattice distortion (or strain) generated during the thermal annealing process [35,36].

To determine how thermal stress affected the luminescent properties of the MHP films, the steady-state PL (Figure 4) and PL lifetime (Figure 5) of the MHP films were measured at different T_{ANN} values. The PL lifetime curves were obtained through TCSPC measurement and were analyzed using a bi-exponential decay model with the equations below [37]:

$$I(t) = A_1 e^{(-t/\tau_1)} + A_2 e^{(-t/\tau_2)},$$

$$\tau_{avg} = f_1\tau_1 + f_2\tau_2 = \frac{A_1\tau_1^2 + A_2\tau_2^2}{A_1\tau_1 + A_2\tau_2}.$$

The short PL lifetime τ_1 (by a fast-decay component), long PL lifetime τ_2 (by a slow-decay component), and average PL lifetime τ_{avg} were summarized with their fractions f_1 and f_2 (intensity-weighted) (Table 4). The bi-exponential decay model is commonly used to fit the PL lifetime curves of the MHP films and to understand the PL decay mechanisms [9,38,39]. As T_{ANN}

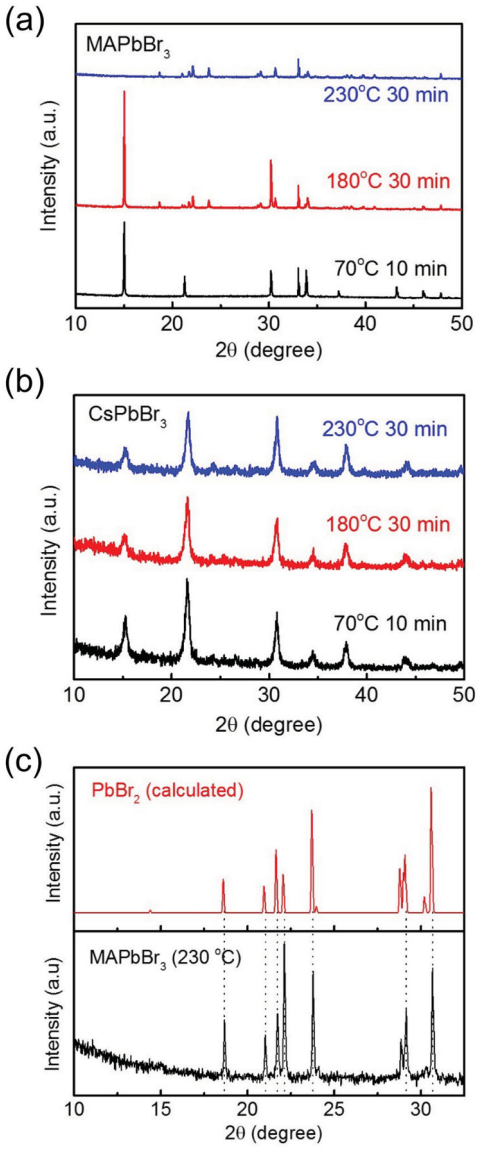

Figure 3. XRD patterns of (a) $MAPbBr_3$ and (b) $CsPbBr_3$ polycrystalline films with different thermal annealing conditions. (c) Magnified XRD pattern of the $MAPbBr_3$ films annealed at 230°C for 30 min (bottom) and calculated pattern of $PbBr_2$ (top) [30].

Table 1. XRD peak positions of the $MAPbBr_3$ polycrystalline films depending on the thermal annealing condition.

	(100)	(110)	(200)	(210)
70°C 10 min	15.02	21.26	30.20	33.86
180°C 30 min	15.02	n.a.	30.22	n.a.
230°C 30 min	n.a.	n.a.	n.a.	n.a.

Note: n.a.: not available because the film was decomposed.

Table 2. XRD peak positions of the $CsPbBr_3$ polycrystalline films depending on the thermal annealing condition.

	(101)	(121)	(202)	(321)
70°C 10 min	15.26	21.58	30.78	37.90
180°C 30 min	15.18	21.64	30.82	37.86
230°C 30 min	15.16	21.72	30.82	37.84

Table 3. Lattice parameters of the $MAPbBr_3$ and $CsPbBr_3$ polycrystalline films depending on the thermal annealing condition.

	Annealing condition	Lattice parameter (Å)		
		$a = b = c$		
$MAPbBr_3$	70°C 10 min	5.891		
	180°C 30 min	5.891		
	230°C 30 min	n.a.		
		a	*b*	*c*
$CsPbBr_3$	70°C 10 min	8.208	11.669	8.195
	180°C 30 min	8.231	11.545	8.257
	230°C 30 min	8.253	11.447	8.257

Note: n.a.: not available because the film was decomposed.

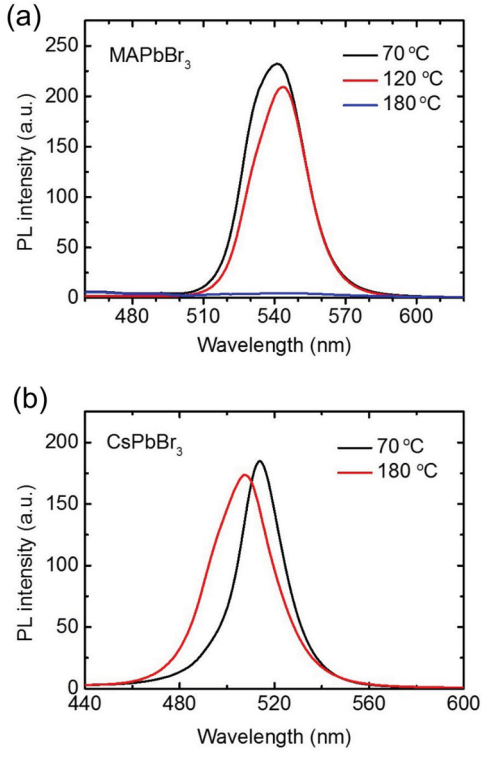

Figure 4. Steady-state PL spectra of the (a) $MAPbBr_3$ and (b) $CsPbBr_3$ polycrystalline films after annealing at 70°C, 120°C, or 180°C for 10 min.

was increased from 70°C to 180°C, the steady-state PL intensity of the $MAPbBr_3$ films decreased; the intensity slightly decreased at $T_{ANN} = 120$°C and became almost negligible at $T_{ANN} = 180$°C (Figure 4(a)). The τ_{avg} of the $MAPbBr_3$ films decreased by ~88% (from 81.5 to 9.6 ns) (Figure 5(a), Table 4). Fraction f_1 of τ_1 was dominant (95%) in the $MAPbBr_3$ film annealed at 180°C (Table 4). In contrast, the PL quenching of the films at the increased T_{ANN} was much less severe in the $CsPbBr_3$ films; the PL intensity of the $CsPbBr_3$ film annealed at 180°C decreased by only ~6% compared with that of the $CsPbBr_3$ film annealed at 70°C (Figure 4(b)). The PL spectrum of the $CsPbBr_3$ film annealed at 180°C was

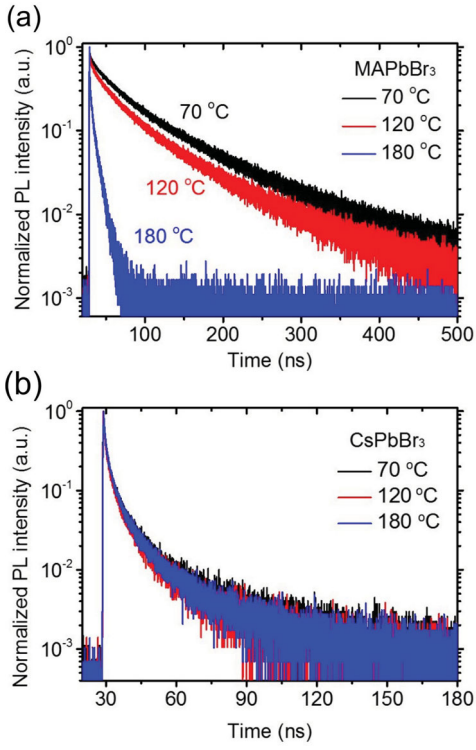

Figure 5. PL lifetime curves of the (a) $MAPbBr_3$ and (b) $CsPbBr_3$ polycrystalline films after annealing at 70°C, 120°C, or 180°C for 10 min.

Table 4. Short PL lifetime (τ_1), long PL lifetime (τ_2), and average lifetime (τ_{avg}) of the $MAPbBr_3$ and $CsPbBr_3$ polycrystalline films depending on T_{ANN} (χ^2 is a statistical measure that evaluates the goodness of fit (the closer χ^2 is to 1, the higher the fitting quality).

	Annealing condition	τ_1 (ns)	f_1 (%)	τ_2 (ns)	f_2 (%)	χ^2	τ_{avg} (ns)
$MAPbBr_3$	70°C 10 min	34.8	41	114.0	59	1.01	81.5
	120°C 10 min	30.0	73	101.0	27	0.89	69.3
	180°C 10 min	7.0	95	59.3	5	0.49	9.6
$CsPbBr_3$	70°C 10 min	6.5	55	39.3	45	0.44	21.1
	120°C 10 min	6.7	58	38.9	42	0.38	20.2
	180°C 10 min	5.7	57	33.1	43	0.40	17.4

blue-shifted and broadened compared with that of the $CsPbBr_3$ film annealed at 70°C. The blue shift and spectral broadening may be ascribed to a change in the ratio of the trap-mediated emission and the band edge emission [40]. This needs to be further investigated in the future studies using transient absorption spectroscopy and a streak camera. The τ_{avg} of the $CsPbBr_3$ films slightly decreased by ~18% (from 21.1 to 17.4 ns) when T_{ANN} increased from 70°C to 180°C (Figure 5(b), Table 4). Furthermore, fractions f_1 and f_2 were almost similar.

The decreases in the PL intensity and τ_{avg} and the increase in the f_1 of the $MAPbBr_3$ films with increasing T_{ANN} can be clearly explained by the thermal decomposition of $MAPbBr_3$, confirmed in the SEM images and XRD patterns (Figures 1 and 2); the destruction of the MHP crystal lattice generates numerous defects that act as trapping sites for charge carriers, and consequently causes trap-assisted non-radiative recombination, which in turn decreases the PL intensity and lifetime [41]. In contrast to $MAPbBr_3$, thermal decomposition did not occur in $CsPbBr_3$ even at T_{ANN} = 230°C, and thereby, the radiative recombination process in $CsPbBr_3$ was not much changed.

4. Conclusion

A comparative study was conducted to determine how the A-site cation affects the thermal stability of MHP polycrystalline films. An OIH MHP ($MAPbBr_3$) and an AI MHP ($CsPbBr_3$) were compared. The $MAPbBr_3$ films were much less thermally stable than $CsPbBr_3$ films; the $MAPbBr_3$ films thermally decomposed into $PbBr_2$ when annealed at $T_{ANN} \geq$ 180°C; the XRD pattern of the $MAPbBr_3$ film annealed at 230°C matched the calculated pattern of $PbBr_2$; i.e. the $MAPbBr_3$ had completely decomposed. The steady-state PL intensity and PL lifetime of the $MAPbBr_3$ films decreased significantly as T_{ANN} increased because the thermal decomposition of $MAPbBr_3$ increases the trap-assisted non-radiative recombination. In contrast, the $CsPbBr_3$ films were not significantly degraded by annealing even at 230°C; the film morphology and XRD patterns were maintained. The steady-state PL intensity and PL lifetime of the $CsPbBr_3$ films were only slightly decreased by annealing at 180°C. These results can provide a way of overcoming the thermal instability of MHPs for application to optoelectronics.

Disclosure statement

No potential conflict of interest was reported by the authors.

Funding

This work was supported by the National Research Foundation of Korea (NRF) grant funded by the Korea government (MSIT) (NRF-2016R1A3B1908431).

Notes on contributors

Himchan Cho received his B.S. (2012.02) and Ph.D. (2016.08) Materials Science and Engineering degrees from Pohang University of Science and Technology (POSTECH), Republic of Korea. He is currently working as a postdoctoral researcher in the Materials Science and Engineering Department, BK21 PLUS SNU Materials Division for Educating Creative Global Leaders of Seoul National University, South Korea (2016.09-present). His

research interests include metal halide perovskites and their application to optoelectronics.

Joo Sung Kim received his B.S. Materials Science and Engineering degree from Pohang University of Science and Technology (POSTECH) in 2016. He is currently pursuing a Ph.D. degree in materials science and engineering at Seoul National University (integrated course). His research interests include organic–inorganic hybrid optoelectronics, organic light-emitting diodes, and spectroscopy.

Young-Hoon Kim received his M.S. (2014) Environmental Science and Engineering and Ph.D. (2016) Material Science and Engineering degrees from Pohang University of Science and Technology (POSTECH), South Korea. He is currently working in the Materials Science and Engineering Department of Seoul National University, South Korea as a postdoctoral researcher (2016–2017). His research focuses on solution-processed electronics based on organic and organic–inorganic hybrid materials for flexible displays and solid-state lighting.

Tae-Woo Lee is an associate professor in the Materials Science and Engineering Department of Seoul National University, South Korea. He received his Ph.D. degree in chemical engineering from KAIST, South Korea in 2002. He joined Bell Laboratories, USA as a postdoctoral researcher, and worked at Samsung Advanced Institute of Technology as a research staff member (2003–2008). He was an associate professor in the Materials Science and Engineering Department of Pohang University of Science and Technology (POSTECH), South Korea until August 2016. His research focuses on printed electronics based on organic and organic–inorganic hybrid materials for flexible displays, solid-state lighting, and solar-energy-conversion devices.

References

[1] Y.-H. Kim, H. Cho, and T.-W. Lee, Proc. Natl. Acad. Sci. U. S. A. **113**, 11694–11702 (2016).

[2] Y.-H. Kim, C. Wolf, Y.-T. Kim, H. Cho, W. Kwon, S. Do, A. Sadhanala, C.G. Park, S.-W. Rhee, S.H. Im, R.H. Friend, and T.-W. Lee, ACS Nano **11**, 6586–6593 (2017).

[3] Y.-H. Kim, G.-H. Lee, Y.-T. Kim, C. Wolf, H.J. Yun, W. Kwon, C.G. Park, and T.-W. Lee, Nano Energy **38**, 51–58 (2017).

[4] J. Pan, L.N. Quan, Y. Zhao, W. Peng, B. Murali, S.P. Sarmah, M. Yuan, L. Sinatra, N.M. Alyami, J. Liu, E. Yassitepe, Z. Yang, O. Voznyy, R. Comin, M.N. Hedhili, O.F. Mohammed, Z.H. Lu, D.H. Kim, E.H. Sargent, and O.M. Bakr, Adv. Mater. **28**, 8718–8725 (2016).

[5] L. Protesescu, S. Yakunin, M.I. Bodnarchuk, F. Krieg, R. Caputo, C.H. Hendon, R.X. Yang, A. Walsh, and M. V. Kovalenko, Nano Lett. **15**, 3692–3696 (2015).

[6] H. Cho, C. Wolf, J.S. Kim, H.J. Yun, J.S. Bae, H. Kim, J.-M. Heo, S. Ahn, and T.-W. Lee, Adv. Mater. **29**, 1700579 (2017).

[7] C. Wolf, J.-S. Kim, and T.-W. Lee, ACS Appl. Mater. Interfaces **9**, 10344–10348 (2017).

[8] A. Sadhanala, F. Deschler, T.H. Thomas, S.E. Dutton, K.C. Goedel, F.C. Hanusch, M.L. Lai, U. Steiner, T. Bein, P. Docampo, D. Cahen, and R.H. Friend, J. Phys. Chem. Lett. **5**, 2501–2505 (2014).

[9] H. Cho, S.-H. Jeong, M.-H. Park, Y.-H. Kim, C. Wolf, C.-L. Lee, J.H. Heo, A. Sadhanala, N. Myoung, S. Yoo, S.H. Im, R.H. Friend, and T.-W. Lee, Science **350**, 1222–1225 (2015).

[10] Y.-H. Kim, H. Cho, J.H. Heo, T.-S. Kim, N. Myoung, C.-L. Lee, S.H. Im, and T.-W. Lee, Adv. Mater. **27**, 1248–1254 (2015).

[11] Z.-K. Tan, R.S. Moghaddam, M.L. Lai, P. Docampo, R. Higler, F. Deschler, M. Price, A. Sadhanala, L.M. Pazos, D. Credgington, F. Hanusch, T. Bein, H.J. Snaith, and R.H. Friend, Nat. Nanotechnol. **9**, 687–692 (2014).

[12] Z. Xiao, R.A. Kerner, L. Zhao, N.L. Tran, K.M. Lee, T.-W. Koh, G.D. Scholes, and B.P. Rand, Nat. Photonics **11**, 108–115 (2017).

[13] M. Yuan, L.N. Quan, R. Comin, G. Walters, R. Sabatini, O. Voznyy, S. Hoogland, Y. Zhao, E.M. Beauregard, P. Kanjanaboos, Z. Lu, D.H. Kim, and E.H. Sargent, Nat. Nanotechnol. **11**, 872–877 (2016).

[14] N. Wang, L. Cheng, R. Ge, S. Zhang, Y. Miao, W. Zou, C. Yi, Y. Sun, Y. Cao, R. Yang, Y. Wei, Q. Guo, Y. Ke, M. Yu, Y. Jin, Y. Liu, Q. Ding, D. Di, L. Yang, G. Xing, H. Tian, C. Jin, F. Gao, R.H. Friend, J. Wang, and W. Huang, Nat. Photonics **10**, 699–704 (2016).

[15] J. Byun, H. Cho, C. Wolf, M. Jang, A. Sadhanala, R.H. Friend, H. Yang, and T.-W. Lee, Adv. Mater. **28**, 7515–7520 (2016).

[16] S.-H. Jeong, S.-H. Woo, T.-H. Han, M.-H. Park, H. Cho, Y.-H. Kim, H. Cho, H. Kim, S. Yoo, and T.-W. Lee, NPG Asia Mater. **9**, e411 (2017).

[17] L. Zhang, X. Yang, Q. Jiang, P. Wang, Z. Yin, X. Zhang, H. Tan, Y.M. Yang, M. Wei, B.R. Sutherland, E.H. Sargent, and J. You, Nat. Commun. **8**, 15640 (2017).

[18] G. Xing, N. Mathews, S.S. Lim, N. Yantara, X. Liu, D. Sabba, M. Grätzel, S. Mhaisalkar, and T.C. Sum, Nat. Mater. **13**, 476–480 (2014).

[19] F. Deschler, M. Price, S. Pathak, L.E. Klintberg, D.D. Jarausch, R. Higler, S. Hüttner, T. Leijtens, S.D. Stranks, H.J. Snaith, M. Atatüre, R.T. Phillips, and R.H. Friend, J. Phys. Chem. Lett. **5**, 1421–1426 (2014).

[20] H. Yuan, E. Debroye, G. Caliandro, K.P.F. Janssen, J. van Loon, C.E.A. Kirschhock, J.A. Martens, J. Hofkens, and M.B.J. Roeffaers, ACS Omega **1**, 148–159 (2016).

[21] S. Lee, J.H. Park, B.R. Lee, E.D. Jung, J.C. Yu, D. Di Nuzzo, R.H. Friend, and M.H. Song, J. Phys. Chem. Lett. **8**, 1784–1792 (2017).

[22] Y.-H. Kim, H. Cho, J.H. Heo, S.H. Im, and T.-W. Lee, Curr. Appl. Phys. **16**, 1069–1074 (2016).

[23] A. Pisoni, J. Jaćimović, O.S. Barišić, M. Spina, R. Gaál, L. Forró, and E. Horváth, J. Phys. Chem. Lett. **5**, 2488–2492 (2014).

[24] M. Kulbak, S. Gupta, N. Kedem, I. Levine, T. Bendikov, G. Hodes, and D. Cahen, J. Phys. Chem. Lett. **7**, 167–172 (2016).

[25] B. Conings, J. Drijkoningen, N. Gauquelin, A. Babayigit, J. D'Haen, L. D'Olieslaeger, A. Ethirajan, J. Verbeeck, J. Manca, E. Mosconi, F. De Angelis, and H.-G. Boyen, Adv. Energy Mater. **5**, 1500477 (2015).
[26] A. Latini, G. Gigli, and A. Ciccioli, Sustain. Energy Fuels **1**, 1351–1357 (2017).
[27] W. Zhu, C. Bao, Y. Wang, F. Li, X. Zhou, J. Yang, B. Lv, X. Wang, T. Yu, and Z. Zou, Dalt. Trans. **45**, 7856–7865 (2016).
[28] B. Roose, A. Ummadisingu, J.-P. Correa-Baena, M. Saliba, A. Hagfeldt, M. Graetzel, U. Steiner, and A. Abate, Nano Energy **39**, 24–29 (2017).
[29] E. Tenuta, C. Zheng, and O. Rubel, Sci. Rep. **6**, 37654 (2016).
[30] M. Lumbreras, J. Protas, S. Jebbari, G.J. Dirksen, and J. Schoonman, Solid State Ionics **20**, 295–304 (1986).
[31] A. Dualeh, N. Tétreault, T. Moehl, P. Gao, M.K. Nazeeruddin, and M. Grätzel, Adv. Funct. Mater. **24**, 3250–3258 (2014).
[32] T. Supasai, N. Rujisamphan, K. Ullrich, A. Chemseddine, and T. Dittrich, Appl. Phys. Lett. **103**, 183906 (2013).
[33] N. Yantara, S. Bhaumik, F. Yan, D. Sabba, H.A. Dewi, N. Mathews, P.P. Boix, H.V. Demir, and S. Mhaisalkar, J. Phys. Chem. Lett. **6**, 4360–4364 (2015).
[34] C.C. Stoumpos, C.D. Malliakas, J.A. Peters, Z. Liu, M. Sebastian, J. Im, T.C. Chasapis, A.C. Wibowo, D.Y. Chung, A.J. Freeman, B.W. Wessels, and M.G. Kanatzidis, Cryst. Growth Des. **13**, 2722–2727 (2013).
[35] J. Zhao, Y. Deng, H. Wei, X. Zheng, Z. Yu, Y. Shao, J.E. Shield, and J. Huang, Sci. Adv. **3**, eaao5616 (2017).
[36] S.R. Raga, M.-C. Jung, M. V. Lee, M.R. Leyden, Y. Kato, and Y. Qi, Chem. Mater. **27**, 1597–1603 (2015).
[37] J.R. Lakowicz, *Principles of Fluorescence Spectroscopy* (Springer Science & Business Media, New York, NY, 2006).
[38] M. Vrućinić, C. Matthiesen, A. Sadhanala, G. Divitini, S. Cacovich, S.E. Dutton, C. Ducati, M. Atatüre, H. Snaith, R.H. Friend, H. Sirringhaus, and F. Deschler, Adv. Sci. **2**, 1500136 (2015).
[39] D. Shi, V. Adinolfi, R. Comin, M. Yuan, E. Alarousu, A. Buin, Y. Chen, S. Hoogland, A. Rothenberger, K. Katsiev, Y. Losovyj, X. Zhang, P.A. Dowben, O.F. Mohammed, E.H. Sargent, and O.M. Bakr, Science **347**, 519–522 (2015).
[40] Q. Han, W. Wu, W. Liu, and Y. Yang, RSC Adv. **7**, 35757–35764 (2017).
[41] A. Al Mamun, T.T. Ava, H.R. Byun, H.J. Jeong, M.S. Jeong, L. Nguyen, C. Gausin, and G. Namkoong, Phys. Chem. Chem. Phys. **19**, 19487–19495 (2017).